Three-dimensional Meso-scopic Analyses of Mortar and Concrete Model by Rigid Body Spring Model

K. Nagai, Y. Sato & T. Ueda
Hokkaido University, Sapporo, Hokkaido, JAPAN

ABSTRACT: Concrete is a heterogeneity material consisting of mortar and aggregate on meso level. Evaluation of fracture process in the meso level is useful to clarify the material characteristic of concrete. However, the mechanical characteristic in the meso level have not been fully understood yet. In this study, three-dimensional analyses of compression and tension test of mortar and compression test of concrete model are carried out by Rigid Body Spring Model (RBSM). In the analyses, fracture process and failure pattern of mortar and the effect of the existence of aggregate in concrete can be simulated qualitatively. These results show the possibility of 3D RBSM analysis to predict the concrete behavior quantitatively in various cases in the future.

Keywords: 3D RBSM, meso-scopic analysis, concrete model, Voronoi geometry

1 INTRODUCTION

Study on concrete on meso level in which concrete is a composite material consisting of mortar and aggregate is useful for the precise evaluation of its material characteristics that are affected by those of components. And also the deterioration of the material characteristics of damaged concrete by an environmental action can be predicted by the analysis from this level in the future.

Many experimental researches were conducted on fracture mechanism on meso level in the past. And in recent years, researches on meso level with the analytical point of view have started but not been fully conducted yet (Asai et al. 2003, Stroeven & Stroeven 2001). Furthermore, discrete three-dimensional analysis is necessary to present the three-dimensional fracture propagation between aggregates three-dimensionally arranged in concrete.

In this study, three-dimensional numerical simulations of fracture process of compression and tension test of mortar and compression test of concrete where shape of the aggregate model is sphere are conducted by 3D Rigid Body Spring Model (RBSM). This analytical method is useful to simulate a discrete behavior like concrete fracture. The authors had developed a two-dimensional RBSM analytical system and constitutive models for mortar and mortar-aggregate interface on meso level (Nagai et al. 2002). The constitutive model for mortar in three-dimensional RBSM is developed in this study based on that in 2D.

2 ANALYTICAL METHOD

The RBSM developed by Kawai (Kawai & Takeuchi 1990) is one of discrete analytical method. Analyzed model is divided into polyhedron elements whose faces are interconnected by springs. Each element has three transitional and three rotational degrees of freedom at the center of gravity. One normal and two shear springs are placed at the center of gravity of each face (Figure 1). Since cracks initiate and propagate along the boundary face, the mesh arrangement may affect fracture direction. To avoid formation of cracks with a certain direction, a random geometry is introduced using a three-dimensional Voronoi diagram (Figure 2). The Voronoi diagram is the collection of Voronoi cells. Each cell represents mortar or aggregate element in the analysis.

In the nonlinear analysis, stiffness matrix is constructed by the principle of virtual work (Kawai & Takeuchi 1990), and the Modified Newton-Raphson method is employed for the convergence calculation. When the model does not converge at the given maximum iterative calculation number, analysis proceeds to next step.

3. CONSTITUTIVE MODEL

3.1 *Mortar model*

In this study, a constitutive model for mortar on meso scale is developed because the constitutive model in macro scale cannot be applied to meso scale analysis.

Material characteristics of each component are presented by means of modeling springs. In normal springs, compressive and tensile stresses (σ) are developed. Shear springs develop shear stresses (τ). For the calculation of shear stress, a resultant value of strains generated in two shear springs is adopted as a shear strain in the constitutive model presented in this section.

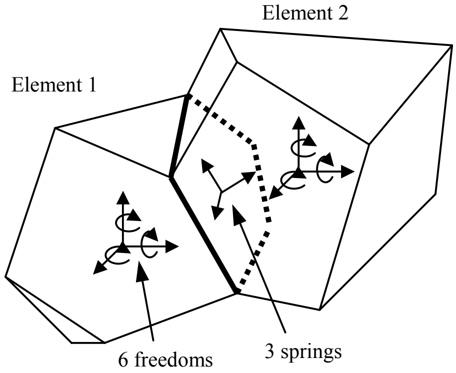

Figure 1. Mechanical model

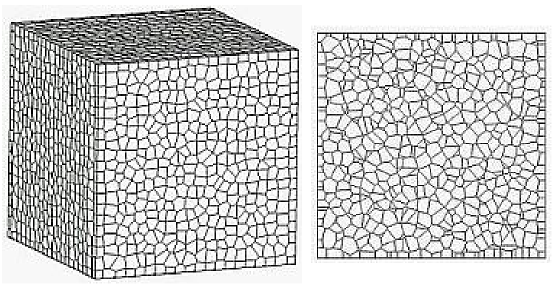

a) 3D view b) Cross section

Figure 2. 3D Voronoi geometry

Elastic modulus of springs are presented assuming plane strain condition,

$$k_n = \frac{(1-\nu_{elem})E_{elem}}{(1-2\nu_{elem})(1+\nu_{elem})}$$
$$k_s = \frac{E_{elem}}{2(1+\nu_{elem})} \quad (1)$$

where k_n and k_s are the elastic modulus of normal and shear spring, E_{elem} and ν_{elem} are the corrected elastic modulus and Poisson's ratio of component for meso level, respectively.

In the analysis, due to the random geometry of the elements, values of the material property, which are the material property on meso level, given to the element are different from those of the analyzed object as the macro-scopic material property. In this study, the material properties for the element were determined in such a way to give the correct macro-scopic properties. For this purpose, the elastic analysis of mortar in compression was carried out. Element fineness of these models was the same level as the models analyzed in the later section. In the elastic analyses, the relationship between the macro-scopic and meso-scopic Poisson's ratio and the effect of the meso-scopic Poisson's ratio on the macro-scopic elastic modulus were examined. From the numerically simulated results, Equations 2 and 3 are adopted for determining the meso-scopic material properties.

$$\nu_{elem} = -237.0\nu^4 + 266.6\nu^3 - 116.1\nu^2 + 24.1\nu - 1.6$$
$$(\ 0.12 < \nu < 0.35\ ) \quad \cdots\cdots \quad (2)$$

$$E_{elem} = \left(-41.5\nu_{elem}{}^4 + 21.1\nu_{elem}{}^3 - 5.5\nu_{elem}{}^2 + 0.4\nu_{elem} + 1.3\right)E \quad \cdots\cdots \quad (3)$$

where E and ν are macro-scopic elastic modulus and Poisson's ratio of component of analyzed object, respectively.

Only the maximum tensile stress has to be set as a material strength. Actually, mortar itself is not a homogeneous material, which is consisting of sand and paste, even when bleeding effect is ignored. However strength distribution in mortar has not been clarified yet. In this study, a normal distribution is assumed for the tensile strength on element boundary. The probability density function is as follows (Figure 3),

$$f(f_{t\,elem}) = \frac{1}{\sqrt{2\pi}} \exp\left\{ -\frac{\{3(f_{t\,elem}/f_{t\,average} - 1)\}^2}{2} \right\} \tag{4}$$

when $f_{t\,elem} < 0$ then,

$$f_{t\,elem} = 0$$

where $f_{t\,elem}$ is distributed tensile strength and $f_{t\,average}$ is average tensile strength of mortar on meso level. And also, the same distribution is given to the elastic modulus. Those distributions affect the macro-scopic elastic modulus, so that the elastic modulus for the element is multiplied by 1.05 to obtain the correct macro-scopic elastic modulus.

Springs set on the face act elastic until generated stresses reach τ_{max} criterion as follows,

$$\begin{aligned} \varepsilon &= \frac{\Delta n}{h_1 + h_2} \\ \gamma &= \frac{\Delta s}{h_1 + h_2} \\ \sigma &= k_n \varepsilon \\ \tau &= k_s \gamma \end{aligned} \tag{5}$$

where ε and γ are the strain of normal and shear springs, respectively. Δn and Δs are the normal and shear relative displacement of elements those compose springs, respectively. *h* is the length of perpendicular line from the center of gravity of element to the boundary. And subscripts 1 and 2 represent elements 1 and 2 in Figure1, respectively. τ_{max} criterion is given as shown in Equation 6 and Figure 4.

$$\tau_{\max} = \pm\left\{0.08 f_{telem}{}^{2.7} \left(-\sigma + f_{telem}\right)^{0.7} + f_{telem}\right\} \quad \left(\sigma < f_{telem}\right) \quad \cdots\cdots \tag{6}$$

When a generated spring stress goes beyond τ_{max}, the shear stress(τ) is reduced to τ_{max} which depends on the normal stress(σ) in the range that the normal stress is less than $f_{t\,elem}$. τ_{max} can increase with increasing normal compressive stress. Stresses can be transferred only through the contact area of each boundary which is calculated by the shear displacement of elements constituting the boundary. Fracture happens between the elements when the normal stress reaches $f_{t\,elem}$, and the normal stress becomes dependent on crack width that is the spring elongation. Shear stress is also affected by the crack width. Both normal and shear stresses are assumed to decrease linearly with the crack width. Stresses after cracking are represented as follows,

$$\begin{aligned} \sigma &= \frac{w_{\max} - w}{w_{\max}} f_{t\,elem} && (w < w_{\max}) \\ \sigma &= 0 && (w \geqq w_{\max}) \\ \tau &= \frac{w_{\max} - w}{w_{\max}} \tau_c && (w < w_{\max}) \\ \tau &= 0 && (w \geqq w_{\max}) \end{aligned} \tag{7}$$

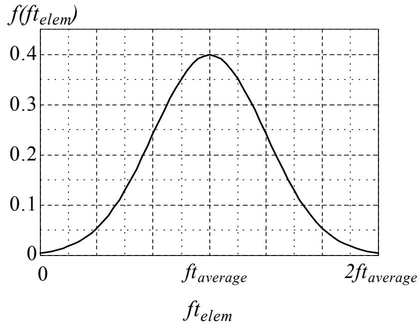

Figure 3. Distribution of material properties

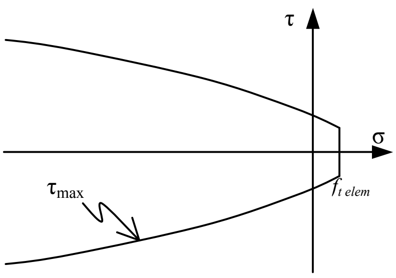

Figure 4. τ_{max} criterion for mortar

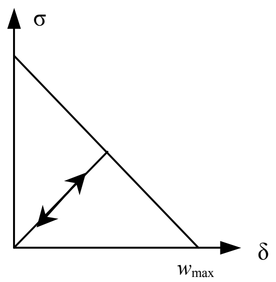

Figure 5. Mortar tensile softening model

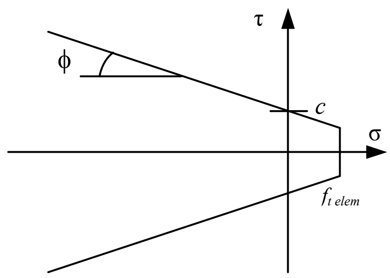

Figure 6. τ_{max} criterion for interface

where,

$$\tau_c = k_s \gamma \qquad (k_s\gamma \leq f_{telem})$$
$$\tau_c = f_{telem} \qquad (k_s\gamma > f_{telem})$$

where w is crack width and w_{max} is the maximum crack width which can carry stress. In this study, w_{max} is set 0.005mm. And the linear unloading and reloading path that goes through the origin is introduced to normal spring in tension softening zone (Figure 5).

In this study, normal springs in compression only behave elastically and never break nor have softening behavior.

3.2 *Aggregate model*

In this study, effect of existence of aggregate in concrete on fracture process is examined. For this purpose, element of aggregate behaves only elastic in this study. The same equations as 1, 2, 3 and 5 are adopted to present the material property of aggregate.

3.3 *Interface model*

The same stress-strain relationships as Equation 5 and strength and stiffness distribution as Equation 4 are adopted for the material properties of the interface between mortar and aggregate. The spring stiffnesses k_n and k_s of the interface are given by a weighted average of the material properties in two elements according to their perpendicular lengths. That is,

$$k_n = \frac{k_{n1}h_1 + k_{n2}h_2}{h_1 + h_2}$$
$$k_s = \frac{k_{s1}h_1 + k_{s2}h_2}{h_1 + h_2} \qquad (8)$$

where subscripts 1 and 2 represent elements 1 and 2 in Figure1, respectively. h is the length of perpendicular line from the center of gravity of element to the boundary. For the interface between mortar and aggregate, the τ_{max} criterion as shown in Equation 9 and Figure 6 is adopted.

$$\tau_{\max} = \pm(-\sigma \tan\phi + c) \qquad (\sigma < f_{telem}) \qquad (9)$$

where ϕ and c are constant values.

This criterion is based on the failure criterion suggested by Kosaka et al (Kosaka et al. 1975) which is derived from experimental results. After stresses reach the failure criterion, the shear stress(τ) is reduced to τ_{max} which depends on the normal stress(σ) in the range where the normal stress is in compression. In tension, both normal and shear stresses cannot transfer the stress after the stresses reach the criterion.

4. ANALYSES OF MORTAR

Numerical analyses of the mortar specimen in compression and tension are carried out. Figure 7 shows 3D view of numerical specimen and x-y cross-section at z=37.5mm. Size of the specimen is 75x75x150mm and number of mortar element is 48,778. Average element size is about 2.59mm^3. In the compression analysis, boundary of top and bottom are fixed in lateral direction. Material properties of mortar are set as shown in Table 1 where only the tensile strength is set as the strength of mortar. Number of the faces in which springs are set is 359,149 in the specimen.

4.1 *Compression analysis*

Figure 8 shows the predicted stress-strain relationships in the mortar compression test. Lateral strains are calculated by the relative deformation between the elements at A and B in Figure 7. Strength of the specimen is 38.87MPa. The strength in compression is 8.7 times bigger than that of in tension (see Section 4.2) and this strength relationship is not far from the experimental results (Nagai et al. 2002). Predicted curves show nonlinearity in axial direction before 50% of maximum stress. Ratio of the lateral strain to the axial strain starts increasing rapidly around 70% of the maximum stress. These behaviors are observed in the experiments of mortar compression test as well (Goble & Cohen 1999, Harsh et al. 1990). Curves in Figure 9 show the number of faces whose crack widths reach 0.002mm, 0.005mm and 0.03mm in the simulation. Horizontal axis shows the macro-scopic strain of the specimen. And also macro-scopic stress is presented in the figure. Number of the faces, whose crack widths become more than 0.005mm and cannot transfer the stresses any more, increases suddenly from around 85% of the maximum stress. This fact that the sudden increase in crack causes the failure of specimen is the same as in usual experimental

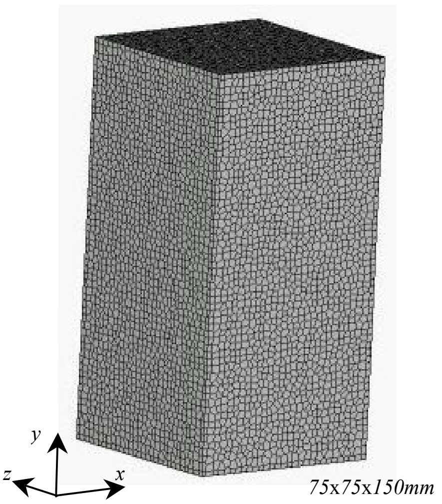

a) 3D view

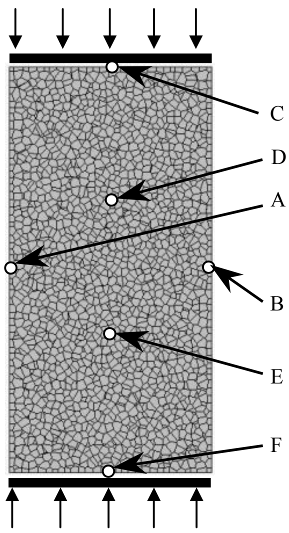

b) Cross-section at z=37.5mm

Figure 7. Numerical specimen

Table 1. Input material properties of mortar

$f_{t\ average}$	4.2 MPa
Elastic modulus (E)	24,000 MPa
Poisson's Ratio (ν)	0.18

results. Figure 10 shows the specimen deformation after peak stress (at axial strain of -2,900μ). Deformations are enlarged 20 times. Failure occurs in other than the vicinity of loading boundary and the damage around the loading boundary is less. This is observed in the case that boundary in lateral direction is fixed (Mier 1997). However, propagation of some main cracks that is observed in the usual experiment

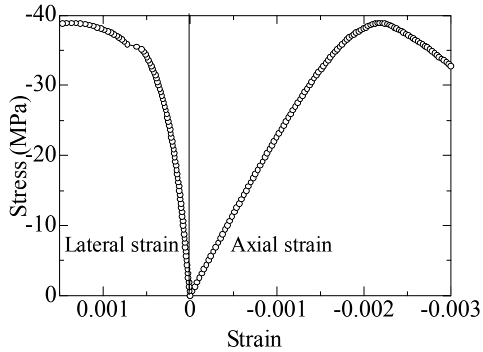

Figure 8. Stress-strain curves in compression

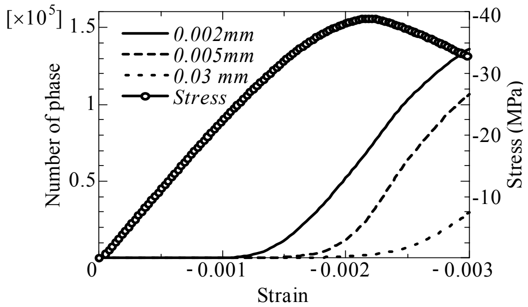

Figure 9. Number of face reaching crack width

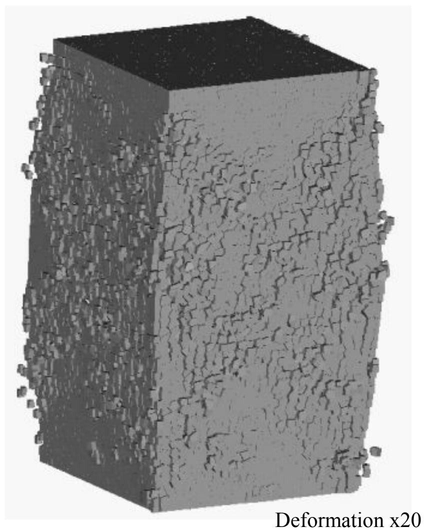

Figure 10. Deformations after peak stress in compression

cannot be simulated in this study.

4.2 *Tension analysis*

Predicted stress-strain relationship in the tension analysis is shown in Figure 11. Macro-scopic tensile strength is 4.47MPa, which is similar to

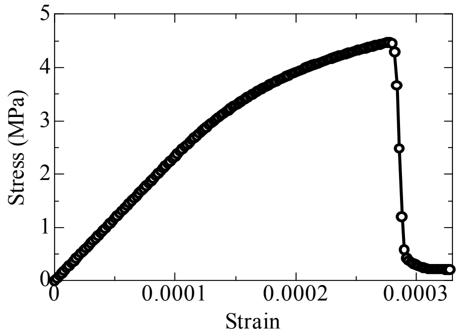

Figure 11. Stress-strain curve in tension

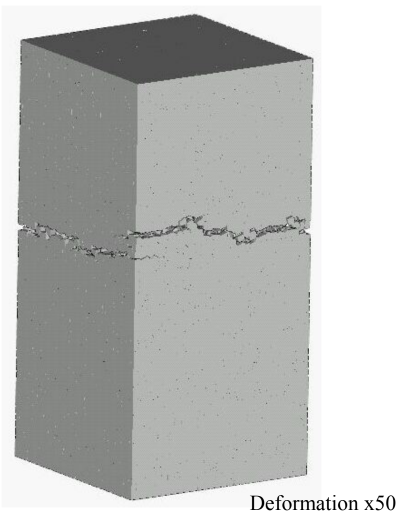

Figure 12. Deformation at failure in tension

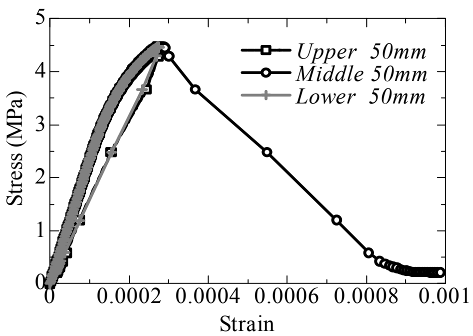

Figure 13. Strains in every 50mm in axial direction

the average tensile strength set on the normal springs (see Section 3.1 and Table 1). The shape of stress-strain curve shows the nonlinearity before the peak stress as much as in compression. This behavior is observed in 2D analysis as well (Nagai et al. 2002). However, experimental evidence shows more linearity in tension. Further research is necessary. Figure 12 shows the deformation of the specimen at failure (at axial strain of 330μ). The deformation is enlarged 50 times. Propagation of single crack that can be seen in usual experiments can be simulated. Figure 13 shows the average strains of every 50mm section in the axial direction. To calculate the strains of *Upper 50mm*, *Middle 50mm* and *Lower 50mm* in Figure 13, relative deformations between the elements at C and D, D and E, and E and F in Figure 7 are used respectively. The vertical axis shows the macro-scopic stress. Until the peak, similar curves are predicted. It means that the specimen extends uniformly. In the post peak range, only the strain in *Middle 50mm* where the single crack propagates (see Figure 12) increases and the strains in other sections reduce. This localization behavior in failure processes in tension is also observed in usual experimental results.

5 ANALYSES OF CONCRETE

Numerical analyses of compression tests of concrete consisting of mortar and sphere aggregates are carried out. Two types of constitutive model for interface between mortar and aggregate are applied to the same specimen to examine the effect of interface bond character: (i) the constitutive model developed in this study (see Section 3.3) – specimen W-BOND; (ii) the constitutive model where only the compressive stress through the normal spring can be transferred and the tensile and shear stresses never be transferred. It means that bond in interface is cut – specimen W/O-BOND.

Sizes of the specimens are 75x75x150mm. Material property of the mortar is same as in the mortar analyses (see Table 1). And the material properties of the aggregate and the interface between mortar and aggregate for specimen W-BOND are presented in Table 2. To determine the material properties of the interface, previous researches (Kosaka et al. 1975, Taylor & Broms 1664, Hsu & Slate 1963) are referred and the general values are selected. Average size of the element is same as the mortar specimen, which is $2.59mm^3$.

Figure 14 shows the numerical model. Aggregate size distribution is determined based on the JSCE Standard Specification for Concrete Structures (JSCE 2002) and the maximum aggregate size is 20mm as shown in Figure 15.

Aggregate diameters used for the analysis are varied with 2mm interval. Number of the aggregates of each size is calculated using the distribution curve in Figure 15 and points on the curve indicate the chosen diameters. Targeted aggregate volume in the model is 35%. However in this study, only the aggregates whose diameters are not less than 10mm are introduced because of the difficulty of forming sphere shape with the small size. Therefore the aggregates those diameter are 8mm are eliminated in numerical model. As a result, the total aggregate volume in the model becomes 24.9%. Table 3 shows the number of the aggregate for each aggregate diameter and total number of aggregate is 167. Loading boundary is fixed in lateral direction for the simulation. Total number of

Table 2. Input material properties

Aggregate	
Elastic modulus (E)	50,000 MPa
Poisson's Ratio (v)	0.25
Interface (for specimen W-BOND)	
$f_{t\ average}$	1.6 MPa
c	2.7 MPa
ϕ	35°

Table 3. Introduced aggregate

Size (mm)	Number
10	72
12	36
14	23
16	16
18	11
20	8
22	1
Total	167

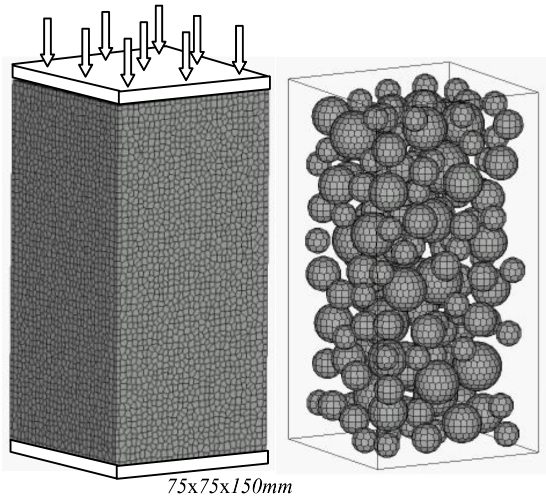

a) 3D view b) Aggregates in the model

Figure 14. Concrete model

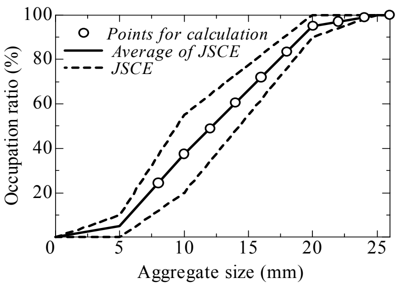

Figure 15. Grain-size distribution

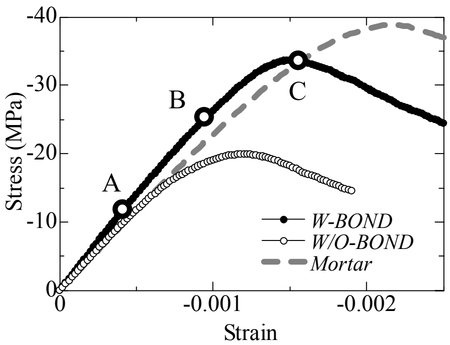

Figure 16. Stress-strain curves

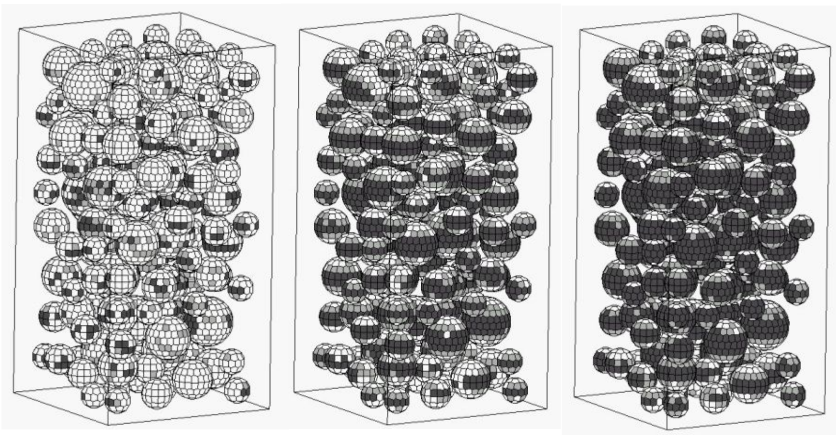

a) Point A b) Point B c) Point C

Face with decreased shear stiffness Cracked face

Figure 17. Changing of condition of the interface

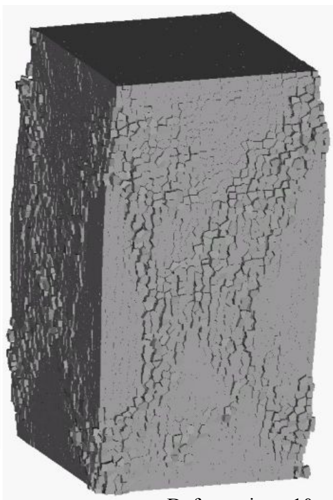

Deformation x10

Figure 18. Deformation at failure

element is 48,258 including 15,867 aggregate elements.

Figure 16 shows the predicted stress-strain curves. The simulated result of mortar is presented as well. Strength of the specimen W-BOND and W/O-BOND are 33.67MPa and 20.01MPa, respectively. Reduction ratio of the strength due to the introduction of aggregates is 13.4% in the case of specimen W-BOND. And it is 48.5% in the case of specimen W/O-BOND. Christensen, P.N. et al. conducted an experiment to examine the effect of bond characteristic of interface (Christensen & Nielsen 1969). In the experiment, two types of sphere aggregate made of glass marble: (i) without coating; (ii) coated by soft layer to cut the bond, were placed in mortar and the compressive test were carried out. In the model that aggregate volume was 20%, the reduction ratios of strength due to the introduction of aggregates were 15% and 40% for the experimental models (i) and (ii) at age 91days, respectively. And in case that aggregate volume was 30%, they were 21% and 54% for the experimental models (i) and (ii), respectively. Though the size of aggregate is difference, these reduction ratios of the strength are similar to the analyses in this study.

Figure 17 shows the change in the interface condition of specimen W-BOND at A-C in Figure 16. Gray and black faces present the faces that reach the τ_{max} criterion in compression and tension, respectively. It means that the decrease of shear stiffness occurs on the gray face and the crack happens on the black face (see Section 3.3). From the Figure 17 a)-c), development of crack band on the side of aggregate is observed and the top and bottom side of aggregate does not have damage. This local behavior on the aggregate surface in failure process of concrete is observed in the experiment (Kosaka et al. 1975, Christensen & Nielsen 1969).

Figure 18 shows the deformation of specimen W-BOND at failure (axial strain of -2,500μ). Deformation is enlarged 10 times. Shear crack can be simulated as in usual experimental results.

6 CONCLUSIONS

The followings are concluded from the analyses of mortar and concrete model by three-dimensional Rigid Body Spring Model (RBSM) with meso scale elements, where only tension and shear failure of spring but no compression failure is assumed.

(1) The calculated stress-strain curves of the mortar in compression show a similar shape to that in usual experimental results.
(2) Sudden increase in number of cracks on meso scale before the peak stress in the compression test of the mortar can be predicted by the analysis.
(3) In the tension analysis of the mortar, the localization of failure after the peak stress and the propagation of single crack can be simulated.
(4) The analysis of concrete can present clearly progressive fracture of the interface between mortar and aggregate. The simulated stress-strain relationship is quite similar to those in usual concrete tests.
(5) Reduction in macro compression strength of the concrete due to inclusion of aggregates and elimination of interface bond can be predicted by the analysis.

7 REFERENCES

Asai, M. et al. 2003. Meso-scopic numerical analysis of concrete structure by a modified lattice model. *J. Struct. Mech. Earthquake Eng., JSCE*, No.731/I-63: 19-30.

Stroeven, P. & Stroeven, M. 2001. Space approach to concrete's space structure and its mechanical properties. *Heron*, Vol.46, No.4: 265-289.

Nagai, K. et al. 2002. Numerical simulation of fracture process of plain concrete by Rigid Body Spring Method. *Proc. of the first fib Congress 2002 Concrete Structures in the 21st Century*, Volume 8: 99-106.

Kawai, T. & Takeuchi, N. 1990. *Discrete limit analysis program, Series of limit analysis by computer 2*. Tokyo: Baihukan. (in Japanese)

Kosaka, Y. et al. 1975. Effect of coarse aggregate on failure process of concrete (report 1 and 2). *Proc. of AIJ*, Vol228: 1-11. (in Japanese)

Goble, C.F. & Cohen, M.D. 1999. Influence of aggregate surface area on mechanical properties of mortar. *ACI Material Journal*, Nov.-Dec.: 657-662.

Harsh, S. et al. 1990. Strain-rate sensitive behavior of cement paste and mortar in compression. *ACI Material Journal*, Sep.-Oct.: 508-516.

Van Mier, J.G.M. 1997. *Fracture process of concrete*. Boca Rton: CRC press.

Taylor, M.A. & Broms, B.B. 1964. Shear bond strength between coarse aggregate and cement paste or mortar. *ACI Journal*, Aug.: 939-956.

Hsu, T.T.C. & Slate, F.O. 1963. Tensile bond strength between aggregate and cement paste or mortar. *ACI Journal*, April: 465-485.

JSCE 2002. *Standard specification for concrete structures - 2002, Materials and construction*. Tokyo: JSCE.

Christensen, P.N. & Nielsen, T.P.H. 1969. Model deformation of the effect of bond between coarse aggregate and mortar on the compressive strength of concrete. *ACI Journal*, Jan.: 69-72.